Phantom dark energy as a natural selection of evolutionary processes â *la genetic algorithm* and cosmological tensions

Mayukh R. Gangopadhyay,[1,*] M. Sami,[1,2,3,†] and Mohit K. Sharma[1,‡]

[1]*Centre For Cosmology and Science Popularization (CCSP), SGT University, Gurugram, Haryana-122505, India*

[2]*Center for Theoretical Physics, Eurasian National University, Astana 010008, Kazakhstan*

[3]*Chinese Academy of Sciences, 52 Sanlihe Rd, Xicheng District, Beijing, China*

(Received 3 July 2023; accepted 25 October 2023; published 21 November 2023)

We study the late-time cosmological tensions using the low-redshift background and redshift-space distortion data by employing a machine learning (ML) technique. By comparing the generated observables with the standard cosmological scenario, our findings indicate support for the phantom nature of dark energy, which ultimately leads to a reduction in the existing tensions. The model-independent approach also enables us to examine the combined background and perturbative history, where tensions are reduced. Moreover, from a statistical perspective, we have shown that our results exhibit a better fit to the data when compared to the ΛCDM model.

DOI: 10.1103/PhysRevD.108.103526

I. INTRODUCTION

One of the major challenges in modern cosmology such as the discrepancies between high-redshift observations of the cosmic microwave background (CMB) [1,2], and low-redshift surveys such as galaxy clustering and weak gravitational lensing [3–6], prompt one to pose a question: *whether the cosmological constant* (Λ) *can be considered a plausible candidate for dark energy (DE)?* As supported by most of the cosmological observations, the ΛCDM model (where CDM refers to the cold dark matter) has recently been subjected to intense scrutiny, particularly with respect to the identification of a high expansion rate and less matter-density clustering in the low-redshift observations. For an instance, low-redshift observations such as Supernovae H_0, for the equation of state of DE (SH0ES) [3] and Kilo Degree Survey (KiDS) [5,6] have challenged Planck-18 estimates for the Hubble constant (H_0) and the matter density clustering ($\sigma_8^{(0)}$) by revealing discrepancies of about 5σ and 3σ, respectively [7–14]. These inconsistencies are not limited to the ΛCDM model but also extend to weakly dynamical dark energy (DE) models that mimics it. As a substantial range of models unable to address these disparities, there are two potential explanations for this: either there exists a systematic error in the data or the ΛCDM model is not a suitable one.

In the literature, many alternative approaches, including those based on modified gravity (MG) theories have investigated the issue by considering the possibility that the ΛCDM model itself may be responsible for these inconsistencies. These approaches includes interactions between dark energy and dark matter [15–17], modifications of gravity at early [18–20] or late times [21–23], distinctive perspective on the dynamic vacuum energy (DVE) concerning the dynamical dark energy [24–28] and so on [10,29–46]. Some of these approaches also consider phenomenologically constructed DE models. However, despite the attempts to explain the low-redshift data, these models often include inherent biases and assumptions. Therefore it can also introduce biases in the estimation of cosmological observables, which may lead to model-specific results rather than the one which can be largely applicable. Due to this potential lack of concordance among several models, the investigation of the tensions necessitates the consideration of a model-independent approach.

In this paper, we adopt a novel model-independent technique that only relies on the data such as the cosmological background and linear perturbative level to study the evolution of the universe. In particular, we use a population-based metaheuristic optimization algorithm that is inspired by the process of natural selection, wherein a fitness function evaluates the fitness (such as the goodness of fit) of individuals (potential solutions) at each step [47–52]. This approach makes use of multiple potential solutions. It ensures that the population (number of solutions) maintains diversity and prevents the optimal solution from becoming trapped in local minima. Once the individuals from the population are selected to reproduce, offspring of the next generation, they may merge together or get themselves

*mayukh_ccsp@sgtuniversity.org

†sami_ccsp@sgtuniversity.org, samijamia@gmail.com

‡mr.mohit254@gmail.com

modified to enhance fitness. This process continues in an effort to emulate the process of natural selection.

To start, we need an initial group of randomly created mathematical functions. Each function in the population is evaluated using a fitness function that measures how well the function fits the given data points. Our approach involves utilizing the χ^2 statistic as the fitness function to assess the "success" of reproducing next generation solutions. After evaluating the fitness of each function in the current population, the ones with higher fitness are selected to become parents for the next generation. Once this step is completed, pairs of different functions take part in crossover to create new functions and the old nodes of the tree gets replaced by the new ones. Mutation is also an essential step in this process because it changes the functions and checks if these changes improve their fitness. The whole process continues until it either reaches the maximum number of generations or when the functions achieve their highest fitness level.

The degree of effectiveness for each solution, which just depends on a single independent variable like redshift, is based on its ability to align with the observational data. The population which minimizes the χ^2 is considered to have the highest fitness. Therefore, our stochastic process aims to proceed in the direction of minimization. It is worth noting that the accuracy of the final optimal solution is largely unaffected by changes in the initial population. Regardless of the initial conditions, the optimization process will generally lead to the same optimal solution, unless any singularities are encountered along the way. The main advantage of using this method is that it can automatically discover most relevant complex features from the data which may be beyond the capability of standard parametric methods.

Our main objective in this paper is to determine if the optimal solution deviates from the ΛCDM model, and if it does, whether it also alleviates the cosmological tension(s). To apply the aforementioned technique to simulate the process of natural selection for the desired observables we intend to use the cosmological background and redshift-space distortion (RSD) data. Since in our approach there are no parameters, so extracting the required DE information from the optimal functional form is highly nontrivial. To determine the cosmological parameters, we choose a cosmological model that encompasses a wide range of DE models and attempt to fit this model to the optimal solution. An advantage of this approach is that when the optimal solution is already identified, the goodness of fit of the optimal solution is typically significantly better than that of the parametric methods. This is due to the predefined functional form in the latter. Once the optimal solution is obtained, a chosen cosmological model can be mapped with it which can essentially provide those fitted parametric values of the model that align with the optimal solution.

The outline of this paper is as follows: First, we study the background expansion rate and then obtain the background optimal solution for the Hubble parameter, we then obtain the corresponding DE equation of state and matter density parameter. Second, we implement the algorithm on the RSD dataset, and obtain the corresponding cosmological parameters. Based on the estimates, we then obtain the bounds on the S_8 parameter. Finally, by using the algorithm assisted optimal solutions for the expansion rate and growth of matter density perturbations we obtain a unified trajectory between them which can be treated as a optimal one in which the tension is reduced or absent.

II. COSMOLOGICAL BACKGROUND EVOLUTION

In this section we will analyze the cosmological background data by using the genetic algorithm (GA) approach. The main objective to consider the GA approach is to remove any biases or the assumptions associated with a chosen cosmological model. This allows one to look for hidden information in the data without encounter the constraints of a cosmological framework. For an example, in the ΛCDM model, the present-day values of the Hubble parameter or the Hubble constant H_0 from the local distance ladder and the cosmic microwave background (CMB) measurements differ by an almost 4σ level. This allows one to reconsider the choice of the ΛCDM model. Hence, without resorting to a particular model, one can have a better understanding of the underlying data. Our main aim is to identify the patterns in the data using a population-based algorithm that can reveal features not easily noticeable in standard cosmological setup. For this reason, we will utilize two different datasets for the background analysis to figure out what does the data actually infer.

Dataset-1: In order to execute the aforementioned algorithm, in this case we use two datasets: (i) Observational Hubble data (OHD) from different redshifts in the range $0.07 < z < 1.965$. In particular, we consider a compilation of $31 H(z)$ measurements obtained from the cosmic chronometric (CC) method (enlisted in [21]). The main reason to use the CC dataset is that it provides direct information about the Hubble parameter at different times (redshifts). This is different from other methods that only measure quantities like luminosity distances etc. without directly studying $H(z)$. (ii) For the SN1a dataset, we make use of the Hubble rate denoted as $E(z) \coloneqq H(z)/H_0$, which consists of six data points within the range of redshift z from 0.07 to 1.5. These six data points effectively contain the information from a larger set of 1048 data points from the Pantheon catalog, as well as 15 data points from the CANDELS and CLASH Multi-Cycle Treasury (MCT) programs obtained by the Hubble Space Telescope (HST). Additionally, based on the arguments presented in the Ref. [53], the data point at $z = 1.5$ has been

excluded from our analysis. The execution of the algorithm is done by incorporating the likelihood function, which is given as

$$L(\chi^2) \propto e^{-\chi^2/2} \quad \text{such that } \chi^2 = \begin{cases} \sum_i \left(\frac{H_{\rm obs}-H_{\rm alg}}{\sigma_i}\right)^2 & \text{For OHD} \\ \sum_{i,j}[E_i - (h_{\rm alg})_i]\cdot c_{ij}^{-1}\cdot[E_i-(h_{\rm alg})_i] & \text{For SN1a,} \end{cases} \tag{1}$$

where $H_{\rm obs}$ and $H_{\rm alg}$ denotes the observed and algorithm fitted Hubble parameter values, respectively, c_{ij} is the covariance matrix, and $h_{\rm alg}$ is the algorithm assisted reduced Hubble parameter.

Dataset-2: This compilation comprises three datasets: (i) 31 measurements of CC, as previously mentioned. (ii) SN1a dataset, for which we utilize the latest and most comprehensive Pantheon + dataset, which includes apparent magnitudes calculated from 1701 light curves representing 1550 SN1a events across a redshift range of z spanning from 0.001 to 2.26, obtained from 18 different surveys. This dataset represents a substantial improvement compared to the initial Pantheon sample of 1048 SN1a events [54], particularly at lower redshift values. The theoretical formula for the apparent magnitude m_B, which is related to the Hubble independent luminosity distance D_L, i.e.,

$$D_L(z) = H_0 d_L(z), \quad \text{where } d_L(z) = (1+z)\int_0^z \frac{d\tilde{z}}{H(\tilde{z})}, \tag{2}$$

can be expressed as

$$m_B(z) = M + 5\log_{10}[D_L(z)] + 5\log_{10}\left(\frac{H_0^{-1}}{1\ \text{Mpc}}\right) + 25, \tag{3}$$

where M is the absolute magnitude of SN. The χ^2 for the SN1a is thus can be written as:

$$\chi^2_{\rm SN} \coloneqq \Delta m_B \cdot C_{\rm SN}^{-1} \cdot \Delta m_B, \tag{4}$$

where $C_{\rm SN}^{-1}$ is the inverse of the SN1a covariance matrix. (iii) The BAO dataset enlisted in [55], includes measurements of various cosmological parameters such as the Hubble distance $D_H(z)$, transverse comoving distance $D_M(z)$, and volume-averaged distance $D_V(z)$. These measurements encompass a redshift range that ranges from 0.38 to 2.334. For this dataset we will adopt the parameter $\Omega_b = 0.02242$ [2] and utilize the sound horizon value at the drag epoch $r_d = 147.78$ Mpc at $z = 1059$ [56]. The corresponding χ^2 is given as:

$$\chi^2_{\rm BAO} = \Delta A \cdot C_{\rm BAO}^{-1} \cdot \Delta A, \tag{5}$$

where A represents the observed quantity. The total χ^2 is thus expressed as:

$$\chi^2_{\rm alg} = \chi^2_{\rm OHD} + \chi^2_{\rm SN} + \chi^2_{\rm BAO}. \tag{6}$$

As one can see that $H_{\rm alg}$ is not defined yet, this is because through the evolutionary process we will try to find its best-fit functional form without assuming any cosmological restrictions. In order to obtain the desired form of $H_{\rm alg}$, we first consider a set of some individuals in the form of mathematical functions such as polynomials, exponentials, etc., which goes through a process of merging and modification. A population of N individuals undergoes combinations after each iteration, and their fitness or likelihood is calculated. Here we note that among the population, individuals with higher fitness are then again considered to generate the new combinations for the next generation, but at the same time, the individuals having lower fitness levels are not excluded from this process. As a result, the algorithm has a tendency to continue searching in the continuous search space in such a way that minor modifications can significantly enhance an individual's fitness. Due to this very reason, one can assure that the final solution does not prematurely converge and approaches the global optima rather than the local one.

For the dataset-1, the best-fit solutions $H_{\rm alg}(z)$ with minimum χ^2 value (corresponds to the maximum fitness) is obtained as[1]:

For OHD:

$$H_{\rm alg}(z) = 72.76 + 68.32z^2 - 13.03z^4 + 0.001z^{15}\ [\text{km/s/Mpc}], \quad \text{with } \chi^2 = 12.58. \tag{7}$$

For OHD+SN1a:

$$H_{\rm alg}(z) = 70.307\exp(0.850z) + 0.769z^8 - 5z^6 - 35.798z\ [\text{km/s/Mpc}], \quad \text{with } \chi^2 = 19.72. \tag{8}$$

Let us here note that for the ΛCDM, the χ^2 value turns around 14.5 for the OHD and 21.19 for OHD+SN1a, therefore our result represents a significant improvement in the fit by about 13% and 7% for OHD and OHD+SN1a,

[1]Here we mention that while the best-fit χ^2 for each run may vary slightly from other runs or require more generations to converge, it consistently yields an almost indistinguishable cosmological evolutionary scenario.

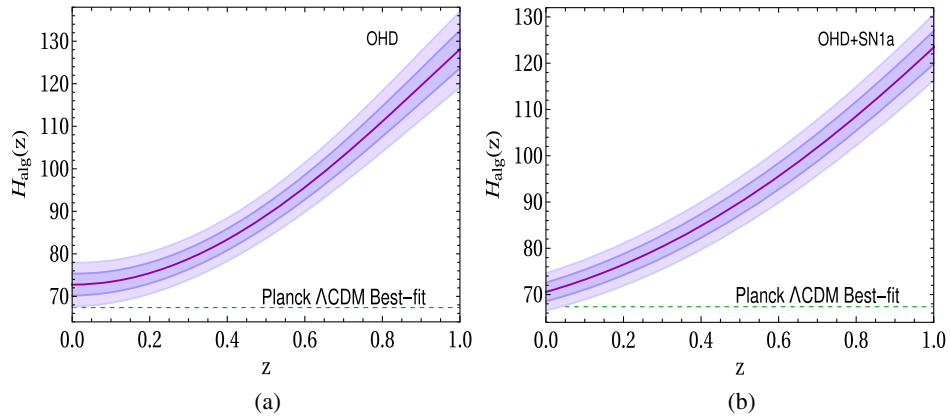

FIG. 1. For Dataset-1, (a) and (b) show the evolutionary profiles of $H_{\rm alg}(z)$ with $z \in [0, 1]$ upto 2σ level for OHD and its combination with the SN1a dataset. The solid line represents the best-fit curve. It clearly shows a notable difference in the Hubble expansion rate when compared to the ΛCDM model, wherein the Hubble rate tends to be comparatively smaller.

respectively.[2] Here, let us emphasize in order to try to decrease variance or overfitting as well as the likelihood of being trapped in the local minima, we have started each run with a significant large population $\sim\mathcal{O}(10^4)$. Also, from Eq. (7) the present-day ($z = 0$) best-fit value for the Hubble parameter ($H_{\rm alg}$) is determined to be 72.76 km/s/Mpc. Since, this best-fit value fits better with the data as compared to the ΛCDM model, it suggests a strong preference for a gravitational modification in the late universe over the ΛCDM and similar cosmological frameworks.

In order to obtain the confidence limits for the above nonparametric best-fit (7) we resort to the bootstrap technique for error estimation. In particular, it generates multiple bootstrap samples by randomly sampling with replacement from the given dataset, and by using them we get the standard deviations or confidence intervals for our observable. The obtained 2σ profiles of $H_{\rm alg}(z)$ with best-fit values are shown in Fig. 1. While the Hubble parameter in Fig. 1(a) does follow the expected trend of decreasing with z at higher redshifts, there is a noticeable deviation around $z \simeq 0.2$ where the decrement of $H_{\rm alg}(z)$ tends to decrease. This contradicts the prediction of various DE models, which suggest that the Hubble parameter will continue to decrease till it becomes almost constant in the far future (which corresponds to the de-Sitter universe). On the other hand, in Fig. 1(b) we show the $H_{\rm alg}(z)$ profile for OHD+SN1a dataset. Here, we observe that the error profile becomes narrower in the latter case, even then it exhibits a tendency toward larger values of H_0. The results of Fig. 1 signals toward the fact that if a particular constituent of the universe, which may be attributed to DE or a result of modified gravity, is intrinsically responsible for the enhancement in $H(z)$ through a positive time-derivative, it could necessarily exhibit a phantomlike behavior [57].

For the dataset-2, we again follow the same procedure to obtain the best-fit functional form of $H_{\rm alg}(z)$ followed by the cosmological parametric values. In this case, we obtain the following:

$$H_{\rm alg}(z) = 70.08(1 + z(0.6715 + 0.22z + 0.005z^2 - 0.029z^3 + 0.01z^4 - 0.0013z^6)^2)\ [\text{km/s/Mpc}], \tag{9}$$

from which one finds that the Hubble constant is 70.08 km/s/Mpc. Whereas, for the ΛCDM, we have obtained the best-fit value of the Hubble constant approximately 68.9 km/s/Mpc. This represents a substantial improvement of $\Delta H(0) = 1.18$ km/s/Mpc in the Hubble constant when compared to the ΛCDM model, thus highlighting its significance in addressing the Hubble tension problem. Furthermore, there is an almost $\Delta\chi^2 = \chi^2_{\Lambda\rm CDM} - \chi^2_{\rm alg} \simeq 2$ improvement compared to the ΛCDM model,

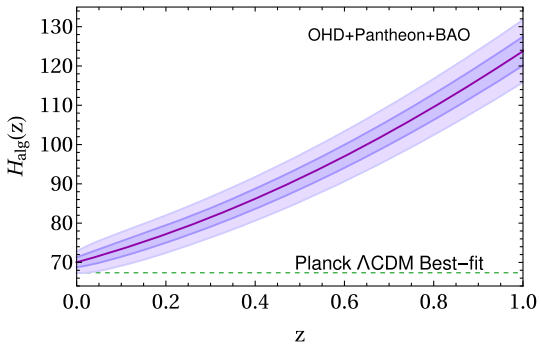

FIG. 2. For dataset-2, the figure show the evolutionary profiles of $H_{\rm alg}(z)$ with $z \in [0, 1]$ upto 2σ level.

[2]It is important to mention that our algorithm's nonparametric nature prevents us from utilizing information criteria like AIC and BIC. These methods impose penalties based on the number of parameters, which is not applicable in our case since our approach does not involve such parameters. Therefore, applying AIC or BIC directly to nonparametric methods is not straightforward because these criteria lack a fixed number of parameters.

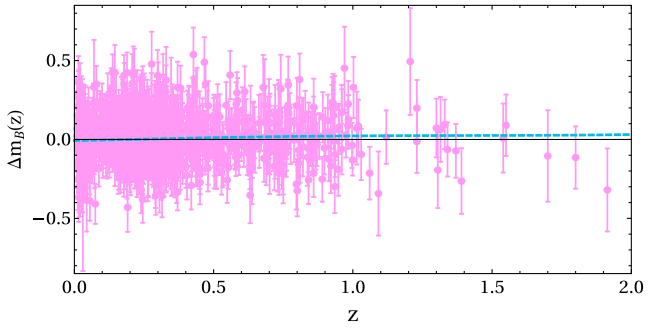

FIG. 3. This figure represents the evolution of $\Delta m_B(z)$ with $z \in [0, 2]$. The error bars correspond to the Pantheon + dataset, and the blue dashed line is the difference between ΛCDM and our best-fit results obtained from the dataset-2.

making our results again more favorable when using the combined dataset. It is also worth emphasizing that due to the chosen Ω_b and r_d that corresponds to the best-fit result of Planck ΛCDM, there is some level of influence of the ΛCDM model in the above obtained form of the $H_{\rm alg}$. Nevertheless, the obtained profile is depicted in Fig. 2, where it is evident that the Planck ΛCDM best-fit falls within a 2σ confidence interval. Notably, the discrepancy with the SH0ES estimate 73.04 ± 1.04 km/s/Mpc has been reduced to within a 2σ level when considering the CC with full Pantheon+ and BAO dataset.

In Fig. 3 we show the observed Δm_B for Pantheon + dataset with up to $z = 2$. The blue-dashed line represents the difference between the apparent magnitudes of for (9) and ΛCDM model. One can see that Δm_B changes sign around $z = 2.5$, preferring slightly small m_B near the current epoch than the concordance model. This is mainly attributed to the fact that $H_{\rm alg} > H_{\Lambda\rm CDM}$ as can be seen from Fig. 2.

To quantitatively measure the effective contribution and dynamical nature of dark energy (DE), it becomes essential to employ a standard Hubble parameter form. However, our approach does not involve any free parameters, which prompts the need to select a specific cosmological framework for estimating the cosmological parameters which corresponds to the above fit. After obtaining the $H(z)$ profiles from two datasets, our next step involves deriving the corresponding cosmological parameters out of it.

A. Cosmological background parameter estimations

To ensure unbiased estimates of the parameters, unaffected by the choice of a specific observable form, we compare the evolution of $H_{\rm alg}(z)$ with the standard framework of the flat-wCDM expression of the Hubble parameter, denoted as $\mathcal{H}(z)$. The comparison between $\mathcal{H}(z)$ and $H_{\rm alg}(z)$ involves the evaluation of parametric and non-parametric forms of the Hubble parameter to deduce the parametric values. It is important to note that direct inference of cosmological parameters like $w_{\rm DE}$ is not feasible from the $H_{\rm alg}$ alone, unless one has the prior knowledge of $\Omega_m^{(0)}$ or $\Omega_{\rm DE}^{(0)}$ values [1]. For a fairly general setup,[3] the Hubble parameter can be written as [58]:

$$\mathcal{H}(z) = H_0\sqrt{\Omega_m^{(0)}(1+z)^3 + (1-\Omega_m^{(0)})(1+z)^{1+w_{\rm DE}}}, \quad (10)$$

where H_0 denotes the Hubble constant, and $\Omega_m^{(0)}$ represents the current density parameter. Assuming a flat universe with pressureless dust, the total equation of state parameter w_T of the system is related to $w_{\rm DE}$ as $w_T = \Omega_{\rm DE} w_{\rm DE}$.

To obtain the values of cosmological parameters that correspond to the best-fit form generated by the algorithm, denoted as $H_{\rm alg}(z)$, we aim to minimize the sum of squared errors, defined as follows:

$$\zeta := \sum_i (H_{\rm alg}(z_i) - \mathcal{H}(z_i))^2, \quad (11)$$

where $z_i \in [0, 1]$ and we divide the range of z into bins of size 0.01. Also, the prior distribution of the parameters are given as:

$$H_0 \in \mathcal{U}[60,80], \quad \Omega_m^{(0)} \in \mathcal{U}[0.2,0.5], \quad w_{\rm DE} \in \mathcal{U}[-1.5,-0.8]. \quad (12)$$

By using the Markov Chain process as a sampling technique we obtain the distribution and best-fit of parameters: $\{H_0, \Omega_m^{(0)}, w_{\rm DE}\}$. It is worth noting that our estimation of H_0 aligns with the findings of direct measurements from the distance-ladder technique, such as SH0ES ($H_0 = 73.04 \pm 1.04$ Km/s/Mpc) and other low-redshift observations such as the Megamaser Cosmology Project (MCP) [59], H_0 Lenses in COSMOGRAIL's Wellspring (H0LiCOW) [4]. These observations measure $H_0 = 73.9 \pm 3$ Km/s/Mpc, and $73.3^{+1.7}_{-1.8}$ Km/s/Mpc, respectively.

Let us emphasize that the significant enhancement in the value of H_0 (as shown in Fig. 4) and the effectively resolution of the Hubble tension can be attributed primarily to the phantom behavior of dark energy, rather than relying on the commonly speculated under-density of matter at low-z [60]. This is due to the fact that in our estimations, the best-fit values of $\Omega_m^{(0)}$ are found to be around 0.35 (see Fig. 4). In fact, the enhancement in H_0 as well as $\Omega_m^{(0)}$ leads to an approximate 6% increase in the total (local) matter density, given by $\Omega_m h^2$, compared to what is predicted from the Planck results. On the other hand, the large negative values of equation-of-state-parameter support the phantom-like nature of DE. In a nutshell, the significant level of

[3]Here we are restricting ourselves for a class of theories which does not take into account the features of dynamical vacuum energy [24–28]. In these cases, the EoS exhibits quintessence or phantom behavior, through by contributions from bosons and fermions in the loop calculation.

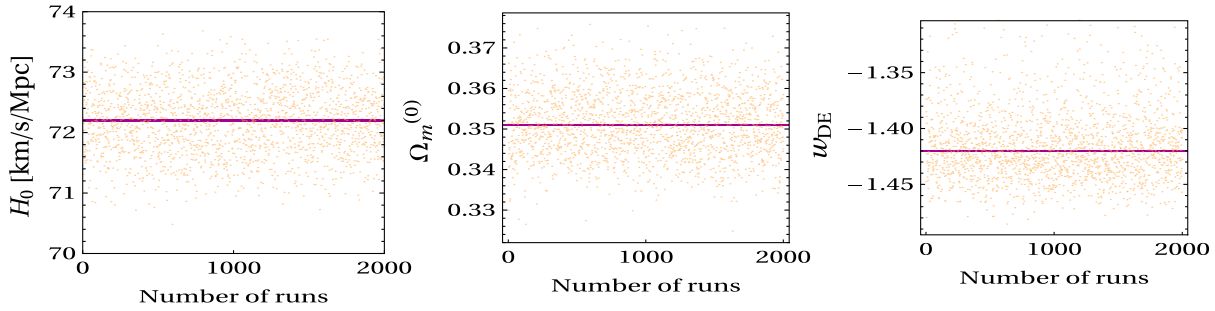

(a) With $H(z)$ data.

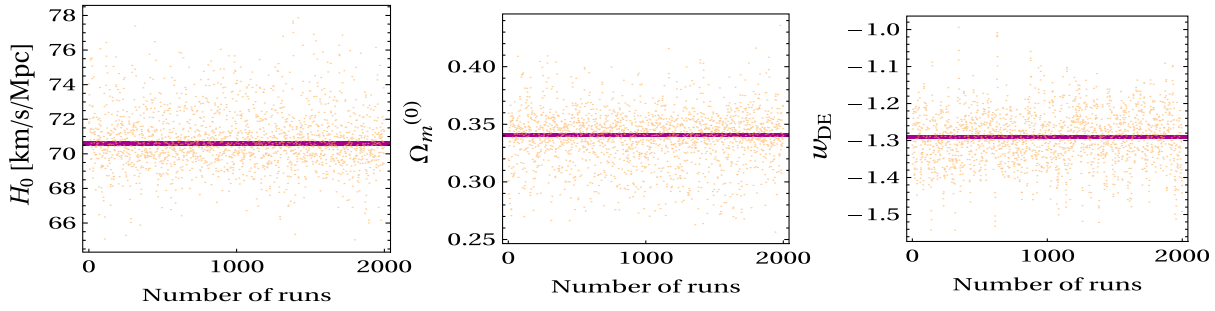

(b) With $H(z)$+SN1a data.

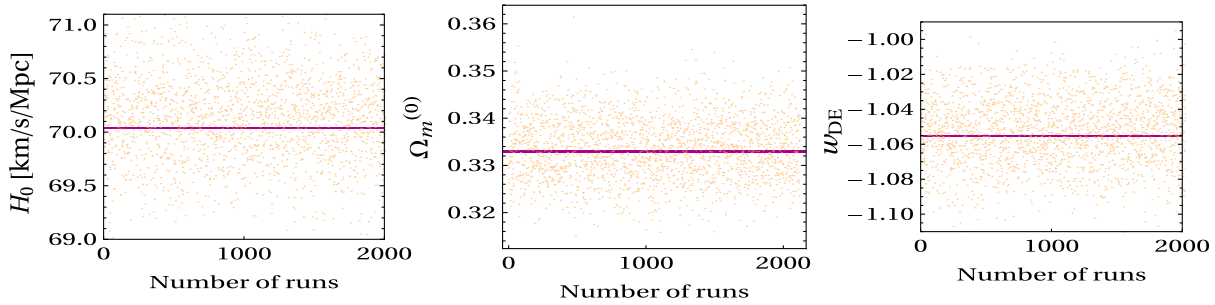

(c) With $H(z)$+Pantheon+BAO.

FIG. 4. (a)–(c) illustrate the parameter values allowed by comparing $H_{\rm alg}(z)$ and $\mathcal{H}(z)$ using the Monte Carlo method for OHD and its combination with SN1a dataset and Pantheon + BAO dataset. The solid line showcase their respective best-fit results.

discrepancy in the measurement of cosmological parameters between parametric and nonparametric methods at the background level is primarily attributed to the inherent biases present in models such as the ΛCDM. If these biases can be mitigated to some extent, the phantom phase, which may not necessarily be mild, aligns more favorably with the observed data.

For the sake of verification, we have also checked the validity of our results, i.e., if the phantomlike behavior is necessarily the reason for the enhancement of the Hubble constant value or is it just the artifact of the choosing wCDM template. In order verify this we consider a more general as well as a theoretically motivated interacting DE-matter scenario which appears in a large class of modified gravity theories. In this scenario, the coupling takes the form of $Q\rho_m\dot{\phi}$ [1], and which does not assume a constant equation-of-state-parameter for DE. In fact, in this case the DE equation of state depends on the coupling as well as on the matter density parameter and is evolving in nature. When compared with the dataset-2 obtained $H_{\rm alg}(z)$ functional form (9), we have found that its corresponding best-fit of $w_{\rm DE}$ is around -1.087, which is even slightly larger than what we have found earlier. This consistency in the results from two different cosmological frameworks with two different sets of background level data indicates that our results are not specific to a given framework. Moreover, our result also corroborate with Ref. [61] where it was shown that in order to alleviate the tension the DE equation of state must reside in the deep phantom regime.

B. Possible physical interpretations of the Hubble parameter form

Let us now look for the conceptual implications of the class of theories to which the Hubble parameter

expressions (7)–(9) may be more closely associated. While these derived expressions are entirely numerical in nature, we have also demonstrated their preference for the phantomlike characteristics of DE. This DE source can potentially originate from single (or multi) field(s) cosmological scenarios, in various class of scalar-tensor equivalent modified gravity theories [62,63]. This characteristic can also appear in disformal coupling between baryonic and dark matter [21,22] which does not assume any extra degrees of freedom. However, identifying which scenario is more preferable to give rise to the algorithm assisted Hubble parameter form at the observational level poses a formidable challenge. Therefore, at this point we can only anticipate that the observed behavior of the Hubble parameter may emerge within some specific, well-defined cosmological scenarios. If it has to be stemmed out within the Einstein frame, there must be atleast two minimally-interacting scalar fields with the matter sector, whether they are in canonical or noncanonical form, such as one considers in the standard quintom scenarios.[4] On the other hand, the phantom nature can also manifest in nonminimally interacting scenarios (or within the Jordan frame), depending upon the chosen coupling(s) between the scalar field and gravity. Furthermore, in disformal coupling scenarios as discussed in [21], it is possible to achieve phantom dark energy behavior when one of the fluids, like baryonic matter, adheres to the geodesic of the Jordan frame, while dark matter follows that of the Einstein frame, and through the disformal coupling it gives rise to phantom DE in the Jordan frame. The model-independent Hubble parameter form allows us to look for a more general cosmological scenario that can address current cosmological tensions. However, determining their consistency with the field equations relies entirely on the specific characteristics of DE. Given that both baryonic and cold dark matter evolve according to $(1+z)^3$, any segment of the observed $H_{\rm alg}(z)$ that remains after subtracting this component can be attributed to the "effective" dark energy for the flat-universe, i.e.,

$$\rho_{\rm DE}(z) \equiv \frac{3H^2_{\rm alg}(z)}{8\pi G_N} - \rho_m(z), \quad \text{where } \rho_m(z) = \rho_m^{(0)}(1+z)^3. \tag{13}$$

It is also worth noting that the various "fitness levels" or the χ^2 involved in the final optimization process may correspond to specific cosmological scenarios, at least those closely approaching the optimal value. For instance, a particular fitness level might align with a specific cosmological model, like quintessence models. However, if it exceeds their fitness, it suggests the possibility of a better theoretical model that can more accurately fit the data.

[4]It is important to highlight that in [27,28] it is shown that the phantom DE may emerge as an effective behavior originating from the quantum vacuum.

III. LINEAR GROWTH RATE OF MATTER DENSITY PERTURBATIONS

Several recent low-z observations of the large-scale structure allow us to figure out the extent of matter density clustering in the universe. In order to analyze it, we utilize the same optimization algorithm to analyze data pertaining to matter perturbation, specifically focusing on redshift-space distortions (RSD). For this dataset, we have used the compilation of $f\sigma_8(z)$ observations, where f is the growth factor of matter perturbations, and σ_8 is the amplitude of power spectrum in $8h^{-1}$ Mpc] [64], and is related to the Power spectrum $P(k)$ via [1]

$$\sigma_8^2 = \frac{1}{2\pi}\int W_s^2 k^2 P(k) dk, \tag{14}$$

where k is the comoving wave number, and W_s is the window function. We consider the growth-gold compilation of $f\sigma_8$ measurements obtained from various galaxy surveys within the redshift interval of $z \in [0.02, 1.94]$ [65]. The main reason for opting for this specific subset of data is due to its uncontaminated nature, lack of anomalies and widely usage (see Refs. [12,34,66]). The χ^2 for the same is defined as:

$$\chi^2 \coloneqq V^i C^{-1}_{ij} V^j, \quad \text{where } V \equiv f\sigma_8(z) - [f\sigma_8(z)]_{\rm alg}, \tag{15}$$

where $[f\sigma_8(z)]_{\rm alg}$ represents the best-fit of the algorithm, and C_{ij} is the covariance matrix between different data points. In line with the background analysis, we have carried out multiple simulations using the identical procedure applied to the cosmological background level. Furthermore, we have also examined various initial values to determine whether the resulting fit exhibit any differences with each other. The best-fit function and it corresponding minimized χ^2 is given as

$$[f\sigma_8]_{\rm alg}(z) = 0.537e^{0.159z} - 10^{-5}z^4 + 0.098z^3 - 0.359z^2 + 0.216z - 0.163, \quad \text{with} \quad \chi^2 = 11.91, \tag{16}$$

For the obtained $[f\sigma_8]_{\rm alg}(z)$ fit, we depict its evolutionary profile up to 1σ level in Fig. 5. Let us note that at the present epoch, Eq. (16) gives

$$[f\sigma_8]_{\rm alg}(0) = 0.374 \pm 0.017, \tag{17}$$

which is significantly lower (a level $> 2\sigma$) than the Planck result of 0.474 ± 0.015. Since in obtaining the result (17)

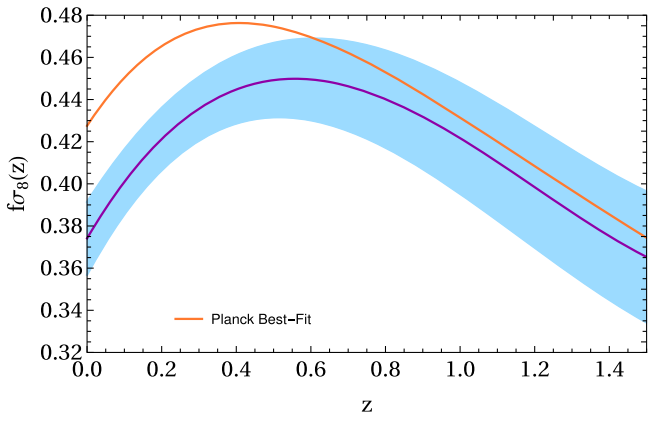

FIG. 5. Optimized growth of matter density clustering with redshift z within the 1σ limit, and Planck's proposed trajectory. Both trajectories merge together at the high-redshifts.

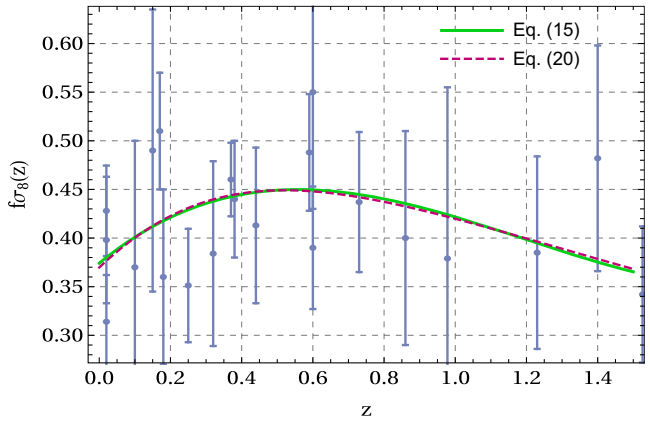

FIG. 6. The figure shows the degree of accuracy in fitting the curve of the wCDM model, using the estimated parameter values (21), with the algorithmically predicted profile of $f\sigma_8(z)$ (16). The solid line represents the predicted profile of $f\sigma_8(z)$ generated by the algorithm, while the dashed line represents the fitting of the wCDM model to the aforementioned prediction. The nearly identical evolutionary patterns of these two curves suggest that our estimates closely match the form generated by the algorithm (16). The corresponding Planck's ΛCDM curve is shown in Fig. 5.

no parametric or functional form was assumed, and it still shows a significant level of tension with the Planck's result, it certainly lead to the conclusion that the discrepancy exists at the level of the observations. As we have observed that the discrepancy in H_0 measurements at the background level is associated with the predominantly phantomlike nature of DE, one may ask: *whether the same parameter reflects a similar discrepancy at the perturbative level?* In order to verify this we will proceed with the same procedure of parameter estimations.

A. Growth rate parameter estimations

In order to comprehend the implications of Fig. 5 in terms of cosmological parameters associated to the growth of matter perturbations, such as $\Omega_m^{(0)}$, $\sigma_8^{(0)}$, and $w_{\rm DE}$, we reconsider the flat-wCDM model. For the latter, the equation of motion of matter density contrast is given by [67]

$$\delta_m'' + \frac{1}{2}[1 - 3(1 - \Omega_m(a))w_{\rm DE}]\delta_m' = \frac{3}{2}\Omega_m\delta_m, \quad (18)$$

where $'$ denotes the derivative with respect to $\log(a)$ and a is the scale factor. In general form, the analytical solution of the matter density contrast δ_m can be found as

$$\frac{\delta_m}{a} = {}_2F_1\left(\frac{w_{\rm DE} - 1}{2w_{\rm DE}}, \frac{-1}{3w_{\rm DE}}; 1 - \frac{5}{6w_{\rm DE}}; a^{-3w_{\rm DE}}\left(1 - \frac{1}{\Omega_m^{(0)}}\right)\right), \quad (19)$$

where ${}_2F_1$ is the Hypergeometric function. Using this one can calculate the theoretical growth rate as

$$f\sigma_8(z) = f(z)\sigma_8^{(0)}\frac{\delta^{(m)}(z)}{\delta^{(m)}(0)}. \quad (20)$$

Here again, we adopt the same approach to statistically compare $f\sigma_8(z)$ with Eq. (20). In particular we try to minimize the squared-difference between the $[f\sigma_8]_{\rm alg}(z)$ and $f\sigma_8(z)$. The estimated values are given as follows[5]:

$$w_{\rm DE} = -1.596 \pm 0.099, \qquad \Omega_m^{(0)} = 0.338 \pm 0.083,$$
$$\sigma_8^{(0)} = 0.795 \pm 0.072. \quad (21)$$

Here also, we see that the equation of state for DE favors its phantom nature by leaning slightly toward lower values (< -1). On the other hand, the value of $\sigma_8^{(0)}$ is significantly higher than what was predicted by low-redshift observations such as KiDS-450 [5] and KiDS-1000 [6]. As already mentioned that the KiDS-450 estimate of $\sigma_8^{(0)} = 0.745 \pm 0.039$ exhibits a tension of more than 2σ with Planck TT, TE, EE + lowE + lensing estimate $\sigma_8^{(0)} = 0.811 \pm 0.006$ [2]. Notably, our estimate on $\sigma_8^{(0)}$ does not show any tension with Planck's $\sigma_8^{(0)}$ result and is in agreement with the latter. In Fig. 6 we depict the accuracy of the best-fit values obtained from the parametric estimations (21) in relation to the algorithm-predicted $f\sigma_8(z)$ profile. The figure demonstrates that the profiles of both the estimations and the algorithm prediction are in alignment, indicating

[5]The obtained minimized χ^2 value is better than that of the corresponding ΛCDM model and the wCDM model. The primary objective of the estimations is to illustrate the potential range of values achievable for the fitting (16).

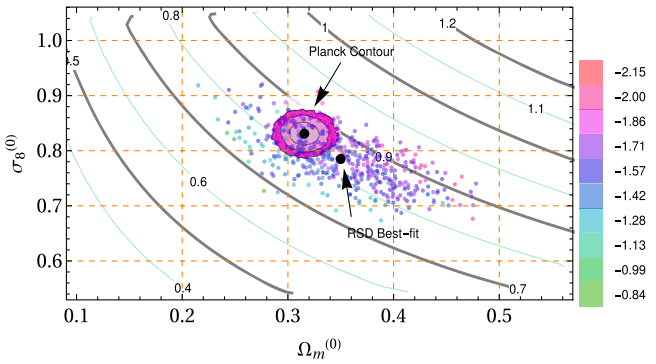

FIG. 7. The figure illustrates the parametric region between $\Omega_m^{(0)}$ and $\sigma_8^{(0)}$, which is allowed based on the Monte Carlo method. The Monte Carlo method generates values distributed normally around the best-fit values (21). The solid region represents the Planck allowed region within a 3σ range. The curved lines in the plot correspond to different values of $S_8^{(0)}$, and the values are indicated on each curve. The color bar on the right side of the figure provides the corresponding values of the equation of state for dark energy for each colored point shown in the plot.

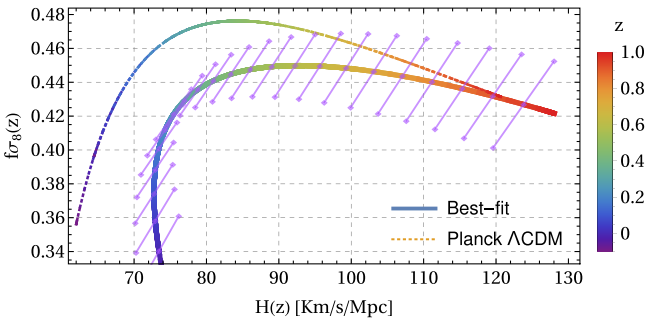

FIG. 8. Evolution of $f\sigma_8(z)$ is shown versus $H(z)$ for $z \in [0, 1]$ for Planck and for our case.

that the estimations (21) are reasonably accurate and exhibit a significant level of goodness of fit.

B. S_8 constraints

The weighted magnitude of matter density perturbations (S_8) captures the degeneracy between $\Omega_m^{(0)}$ and $\sigma_8^{(0)}$ and is formulated as [66]:

$$S_8^{(0)} = \sigma_8^{(0)} \sqrt{\frac{\Omega_m^{(0)}}{0.3}}. \tag{22}$$

In the framework of the ΛCDM model, measurements of CMB anisotropy by the Planck 2018 have yielded $S_8^{(0)} = 0.834 \pm 0.016$ [2]. In contrast, a number of surveys of RSD consistently suggests $S_8^{(0)}$ values that tend to be lower than those inferred from CMB measurements, falling within the range of [0.703, 0.782]. However, when using the estimates (21) in Eq. (22), and using the error-propagation technique, we find

$$S_8^{(0)} = 0.833 \pm 0.188, \tag{23}$$

for the RSD dataset shown in Fig. 7. This indicates a notable increase in the value of $S_8^{(0)}$ (although with a considerable level of uncertainty) and approaches the estimation by Planck $\mathrm{TT, TE, EE + lowE}$ of $S_8^{(0)} = 0.834 \pm 0.016$ [2]. This suggests that if not be due to systematics, any disagreement or tension between the high and low redshift data might be due to the choice of the cosmological model which is used to describe the universe at late times.

IV. JOINT BACKGROUND AND PERTURBATIVE LEVEL EVOLUTION

As we have earlier shown that in order to address the tension at both the background and linear perturbative levels, it is important to deviate from the standard ΛCDM model toward a more phantomlike behavior. It is also important to note that both the estimates obtained from background and perturbative level data for parameters such as $\Omega_m^{(0)}$ and w_{DE} are consistent with each other. This indicates that both sets of data align with each other and allow us to find a unified trajectory for the evolutionary history of the universe, accounting for both the growth of large-scale structure and the rate of expansion. Therefore, by using the Eqs. (7) and (16), we can analyze how the quantities $[f\sigma_8]_{\mathrm{alg}}(z)$ and $H_{\mathrm{alg}}(z)$ change together over a range of redshifts. This will give us the hint for the possible evolutionary profile of the universe which is required for reducing or rather resolving the existing tensions between the measurements. It will also allow us to examine the joint background and perturbative evolution of the universe without being limited by any constraints on the parameter.

The obtained profile is shown in Fig. 8 in which we have also depicted the evolution of linear perturbation with the background expansion by utilizing the Planck $\mathrm{TT, TE, EE + lowE + lensing}$ best-fits (dotted curve) with $\Omega_m^{(0)} = 0.315$ and $\sigma_8^{(0)} = 0.8111$ [2]. The figure illustrates that both trajectories (fitted one and that correspond to the Planck's best-fit) have followed similar behavior in the past. However, a noticeable deviation from each other is observed at $z \leq 0.4$. Also, the growth rate of matter perturbations for the Planck tends to be less suppressed than our case, and therefore reaches a peak value that is higher than what is predicted by our analysis almost at the same redshift value.

As we have seen that the joint evolution of $f\sigma_8(z)$ and $H(z)$ is unique in the sense that it corresponds to those cosmological parametric values at the current epoch which relieves the tensions. This is in contrast to most scenarios where the particular correlation between the H_0 and $\sigma_8^{(0)}$ estimates for a given model tends to worsen the one while solving the other.

To assess the compatibility between the two observables, namely $H(z)$ and $f\sigma_8(z)$, and to determine the profile suggested by the background data for $f\sigma_8(z)$, one needs to know the background parameters, such as $\Omega_m^{(0)}$ and $w_{\rm DE}$, to use in Eq. (18). By utilizing the best-fitting values of the background parameters obtained in Sec. II A in Eq. (20), and comparing it with the $f\sigma_8(z)$ profile derived from the RSD data estimations (21), we find $\sigma_8^{(0)} \simeq 0.77$. This value is in agreement with the estimated value given in Eq. (21). Consequently, our background and perturbative-level analyses align with each other, indicating consistency in our results.

In order to assess whether the $f\sigma_8(z)$ profiles obtained from the background data estimations are compatible with the one that is obtained using the RSD dataset, we use a simple technique that calculates the area between any two functional profiles. The area which denotes the divergence between two profiles is given by $A = \int_z |f(z) - g(z)|dz$. Hence, larger the area the less compatibility between two profiles, or vice-versa. After applying this technique, we have found that the value of A for the estimations (21) and the background estimations (II A) is approximately $\mathcal{O}(10^{-3})$, whereas when compared with the ΛCDM estimations, A is of the order of $\mathcal{O}(10^{-2})$. The comparatively large compatibility between our background and linear perturbative-level estimations agrees to the fact that there is a significant level of deviation from the ΛCDM model toward the phantom.

V. CONCLUSION

We have conducted two comprehensive independent analyses to identify the reasons behind two tensions related to parameters H_0 and $\sigma_8^{(0)}$ using a metaheuristic optimization technique. To determine the necessary requirement(s) that align(s) most favorably with the optimized form of the observables obtained by our algorithm, we have chosen the wCDM model for simplicity. However, we have also demonstrated that the outcomes are also consistent with interacting dark energy scenarios. Notable, our cosmological model-agnostic findings have demonstrated that the phantom nature of a dynamical DE is required to relax both of the tensions. We have also shown that in order to tackle both the tensions together a specific profile of a trajectory between $H(z) - f\sigma_8$ is required.

Regarding the background evolution, we have obtained the fitting using the metaheuristic optimization algorithm for the $H(z)$ for two separate cases to figure out if the results are indeed pointing toward the same physics or not. Hence, in first analysis we take distance-ladder measurements and its combination with SN1a dataset, and in the second case we take the combination of the former with full Pantheon+ and BAO dataset. After obtaining the optimized functional form of $H_{\rm alg}(z)$ from the simulation, we have then searched for the corresponding cosmological scenario, which can or at least try to resemble it. For the purpose of estimation, we choose wCDM model, and with multiple simulations, we have obtained an average values for the same, which correspond to the optimized fitting profiles of $H(z)$. We have explicitly shown that because of the natural emergence of the phantom nature of DE the H_0 tension is relaxed/reduced in CCH and its combination with SN1a dataset and BAO dataset. Here we also want to mention that for the CC+SN1a+BAO dataset the observed mild phantom behavior indicated by the dark energy equation of state, denoted as $w_{\rm DE} = -1.087$, is primarily a result of fixing the sound horizon to the best-fit value of the ΛCDM model for the BAO dataset. As a result, this significant biasing effect effectively limits the degree to which the CC+SN1a dataset can penetrate into the phantom regime. The extent to which phantom nature can exhibit without the BAO dataset has been explicitly demonstrated by our use of the CC+SN1a dataset in the case of dataset-1. Moreover, our overall conclusion is in contrast to the point of view that the tension might be due to the low-matter density in the universe. This is due to the fact that in all different set of combinations of dataset, we have found $\Omega_m^{(0)} \in [0.33, 0.35]$. Since the corresponding results agree with both sets of data thereby establishing their reliability, while having the potential to alleviate/reduce the H_0 tension. Here it is also important to mention that late-time modifications or considering the alternatives of ΛCDM are necessary due to the fact that the early-time possible resolutions for tackling the Hubble tension suffers with various issues and does not fully resolve the tension [20].

As to the linear growth of matter density perturbations, we have carried out a similar procedure for finding out the cosmological parameters using RSD dataset. Here also, we have shown that the corresponding optimized fitting surpasses the fitting of the ΛCDM by a significant margin. We have then obtained the corresponding parameters using the latter and it strongly supports the phantom nature of DE. It is also in tune with the large $\sigma_8^{(0)}$ value, which eventually reduces the tension. Furthermore, by using the obtained constraints, we have constrained the $S_8^{(0)}$ parameter and showed that its best-fit also lies toward the Planck's estimate. We have also shown that our results obtained using RSD dataset are compatible with the background ones. In summary, we have shown that both at the background and linear perturbative levels, the tensions can be alleviated if one chooses a suitable candidate for DE which exhibits a phantom nature at late times.

Let us emphasise that our analysis, which involves multiple datasets and their combinations, consistently demonstrates a better fit when compared to the ΛCDM model. This suggests the potential necessity for DE to exhibit phantomlike behavior. Furthermore, aligning the model-independent observables with two distinct cosmological templates strengthens our argument. This approach is better in the sense that it allows us to obtain even small features of the observables in the data without relying on initial model-dependent assumptions.

There are still some unanswered questions that remain: (i) What insights can the optimized fitting provide regarding the interaction between dark energy (DE) and matter? (ii) If a model is capable of reproducing the corresponding results, will it exhibit stability? (iii) What will happen if the sound horizon is not fixed in prior? We are looking forward to answering these questions and trying to report on them in the near future.

ACKNOWLEDGMENTS

We thank Savvas Nesseris, Eoin O. Colgain, and Maurice VanPutten for their fruitful discussions on the draft. We also thank the anonymous reviewer for careful reading of our manuscript and giving many insightful comments and suggestions. The work of M. R. G. is supported by DST, Government of India under the Grant Agreement Number IF18-PH-228 (Inspire Faculty Award). The work of M. R. G. and M. S. is supported by Science and Engineering Research Board (SERB), DST, Government of India under the Grant Agreement Number CRG/2022/004120 (Core Research Grant). M. S. is also partially supported by the Ministry of Education and Science of the Republic of Kazakhstan, Grant No. AP14870191 and CAS President's International Fellowship Initiative (PIFI).

[1] L. Amendola and S. Tsujikawa, *Dark Energy: Theory and Observations* (Cambridge University Press, United Kingdom, 2010).
[2] N. Aghanim *et al.*, Planck 2018 results. VI. Cosmological parameters, Astron. Astrophys. **641**, A6 (2020).
[3] A. G. Riess *et al.*, A 2.4% determination of the local value of the Hubble constant, Astrophys. J. **826**, 56 (2016).
[4] K. C. Wong *et al.*, H0LiCOW—XIII. A 2.4 per cent measurement of H0 from lensed quasars: 5.3σ tension between early- and late-universe probes, Mon. Not. R. Astron. Soc. **498**, 1420 (2020).
[5] H. Hildebrandt *et al.*, KiDS-450: Cosmological parameter constraints from tomographic weak gravitational lensing, Mon. Not. R. Astron. Soc. **465**, 1454 (2017).
[6] C. Heymans *et al.*, KiDS-1000 cosmology: Multi-probe weak gravitational lensing and spectroscopic galaxy clustering constraints, Astron. Astrophys. **646**, A140 (2021).
[7] E. Di Valentino *et al.*, Cosmology intertwined III: $f\sigma_8$ and S_8, Astropart. Phys. **131**, 102604 (2021).
[8] E. Di Valentino, O. Mena, S. Pan, L. Visinelli, W. Yang, A. Melchiorri, D. F. Mota, A. G. Riess, and J. Silk, In the realm of the Hubble tension—A review of solutions, Classical Quantum Gravity **38**, 153001 (2021).
[9] J. Solà Peracaula, A. Gomez-Valent, J. de C. Perez, and C. M.-Pulido, Running vacuum in the Universe: Phenomenological status in light of the latest observations, and its impact on the σ_8 and H_0 tensions, Universe **9**, 262 (2023).
[10] M. G. Dainotti, G. Bargiacchi, M. Bogdan, S. Capozziello, and S. Nagataki, Reduced uncertainties up to 43% on the Hubble constant and the matter density with the SNe Ia with a new statistical analysis, arXiv:2303.06974.
[11] G. Bargiacchi, M. G. Dainotti, and S. Capozziello, Tensions with the flat ΛCDM model from high-redshift cosmography, Mon. Not. R. Astron. Soc. **525**, 3104 (2023).
[12] R. D'Agostino and R. C. Nunes, Cosmographic view on the H0 and $\sigma 8$ tensions, Phys. Rev. D **108**, 023523 (2023).
[13] J. de C. Perez, J. Solà Peracaula, and C. P. Singh, Running vacuum in Brans-Dicke theory: A possible cure for the σ_8 and H_0 tensions, arXiv:2302.04807.
[14] N. Nguyen, D. Huterer, and Y. Wen, Evidence for suppression of structure growth in the concordance cosmological model, Phys. Rev. Lett. **131**, 111001 (2023).
[15] B. J. Barros and L. Amendola, and T. Barreiro, and N. J. Nunes, Coupled quintessence with a ΛCDM background: Removing the σ_8 tension, J. Cosmol. Astropart. Phys. 01 (2019) 007.
[16] J. B. Jiménez, D. Bettoni, D. Figueruelo, F. A. T. Pannia, and S. Tsujikawa, Probing elastic interactions in the dark sector and the role of S_8, Phys. Rev. D **104**, 103503 (2021).
[17] K. L. Pandey, T. Karwal, and S. Das, Alleviating the H_0 and σ_8 anomalies with a decaying dark matter model, J. Cosmol. Astropart. Phys. 07 (2020) 026.
[18] M. C. Carrillo, Mariana, Q. Liang, and J. Sakstein, and M. Trodden, Neutrino-assisted early dark energy is a natural resolution of the Hubble tension, arXiv:2302.09091.
[19] J. Sakstein and M. Trodden, Early dark energy from massive neutrinos as a natural resolution of the Hubble tension, Phys. Rev. Lett. **124**, 161301 (2020).
[20] S. Vagnozzi, Seven hints that early-time new physics alone is not sufficient to solve the Hubble tension, Universe **9**, 393 (2023).
[21] S. A. Adil, M. R. Gangopadhyay, M. Sami, and M. K. Sharma, Late-time acceleration due to a generic modification of gravity and the Hubble tension, Phys. Rev. D **104**, 103534 (2021).
[22] M. R. Gangopadhyay, S. K. J. Pacif, M. Sami, and M. K. Sharma, Generic modification of gravity, late time acceleration and Hubble tension, Universe **9**, 83 (2023).
[23] G. Montani, M. De Angelis, F. Bombacigno, and N. Carlevaro, Metric $f(R)$ gravity with dynamical dark energy as a paradigm for the Hubble Tension, arXiv:2306.11101.
[24] J. Solà Peracaula, A. Gómez-Valent, J. de C. Perez, and C. Moreno-Pulido, Running vacuum against the H_0 and σ_8 tensions, Europhys. Lett. **134**, 19001 (2021).

[25] J. Solà Peracaula, A. Gómez-Valent, J. de C. Perez, and C. Moreno-Pulido, Running vacuum in the universe: Phenomenological status in light of the latest observations, and its impact on the σ_8 and H_0 tensions, Universe **9**, 262 (2023).
[26] C. Moreno-Pulido and J. Solà Peracaula, Renormalizing the vacuum energy in cosmological spacetime: Implications for the cosmological constant problem, Eur. Phys. J. C **82**, 551 (2022).
[27] C. Moreno-Pulido and J. Solà Peracaula, Equation of state of the running vacuum, Eur. Phys. J. C **82**, 137 (2022).
[28] C. Moreno-Pulido, J. Solà Peracaula, and S. Cheraghchi, Running vacuum in QFT in FLRW spacetime: The dynamics of $\rho_{\rm vac}(H)$ from the quantized matter fields, Eur. Phys. J. C **83**, 637 (2023).
[29] E. D. Valentino, A. Melchiorri, and J. Silk, Planck evidence for a closed Universe and a possible crisis for cosmology, Nat. Astron. **4**, 196 (2019).
[30] E. Abdalla, Cosmology intertwined: A review of the particle physics, astrophysics, and cosmology associated with the cosmological tensions and anomalies, J. High Energy Astrophys. **34**, 49 (2022).
[31] E, D. Valentino *et al.*, Cosmology intertwined III: $f\sigma_8$ and S_8, Astropart. Phys. **131**, 102604 (2021).
[32] V. Poulin, J. L. Bernal, E. Kovetz, and M. Kamionkowski, The sigma-8 tension is a drag, Phys. Rev. D **107**, 123538 (2023).
[33] K. Jedamzik and L. Pogosian, Relieving the Hubble tension with primordial magnetic fields, Phys. Rev. Lett. **125**, 181302 (2020).
[34] G. Alestas and L. Perivolaropoulos, Late-time approaches to the Hubble tension deforming H(z), worsen the growth tension, Mon. Not. R. Astron. Soc. **504**, 3956 (2021).
[35] R. Shah, A. Bhaumik, P. Mukherjee, and S. Pal, A thorough investigation of the prospects of eLISA in addressing the Hubble tension: Fisher forecast, MCMC and machine learning, J. Cosmol. Astropart. Phys. 06 (2023) 038.
[36] R. Arjona and S. Nesseris, What can machine learning tell us about the background expansion of the universe?, Phys. Rev. D **101**, 123525 (2020).
[37] R. Arjona and S. Nesseris, Hints of dark energy anisotropic stress using machine learning, J. Cosmol. Astropart. Phys. 11 (2020) 042.
[38] E. O. Colgáin, M. H. P. M. van Putten, and H. Yavartanoo, De Sitter swampland, H_0 tension and observation, Phys. Lett. B **793**, 126 (2019).
[39] D. H. F. de Souza and R. Rosenfeld, Can neutrino-assisted early dark energy models ameliorate the H_0 tension in a natural way?, Phys. Rev. D **108**, 083512 (2023).
[40] G. Garcia-Arroyo, J. L. Cervantes-Cota, and U. Nucamendi, Neutrino mass and kinetic gravity braiding degeneracies, J. Cosmol. Astropart. Phys. 08 (2022) 009.
[41] M. H. Chan, The cosmological ultra-low frequency radio background: A solution to the Hubble tension and the 21-cm excess trough, Eur. Phys. J. C **83**, 509 (2023).
[42] P. D. Meerburg, Alleviating the tension at low-l through axion monodromy, Phys. Rev. D **90**, 063529 (2014).
[43] S. J. Clark, K. Vattis, J. Fan, and S. M. Koushiappas, H_0 and S_8 tensions necessitate early and late time changes to ΛCDM, Phys. Rev. D **107**, 083527 (2023).
[44] A. Alexandra and G. Efstathiou, A non-linear solution to the S_8 tension?, Mon. Not. R. Astron. Soc. **516**, 5355 (2022).
[45] L. Kazantzidis and L. Perivolaropoulos, Evolution of the $f\sigma_8$ tension with the Planck 15/ΛCDM determination and implications for modified gravity theories, Phys. Rev. D **97**, 103503 (2018).
[46] S. Basilakos, A. Lymperis, M. Petronikolou, and E. N. Saridakis, Alleviating both H_0 and σ_8 tensions in Tsallis cosmology, arXiv:2308.01200.
[47] S. Mirjalili, *Evolutionary Algorithms and Neural Networks: Theory and Applications*, Studies in Computational Intelligence Vol. 780 (Springer, Berlin/Heidelberg, Germany, 2019).
[48] J. H. Holland, Genetic algorithms, Sci. Am. **267**, 66 (1992).
[49] O. Kramer and O. Kramer, *Genetic Algorithms* (Springer International Publishing, New York, 2017).
[50] J. Liesenborgs, S. De Rijcke, and H. Dejonghe, A genetic algorithm for the non-parametric inversion of strong lensing systems, Mon. Not. R. Astron. Soc. **367**, 1209 (2006).
[51] S. A. Abel, A. Constantin, T. R. Harvey, and A. Lukas, Cosmic inflation and genetic algorithms, Fortschr. Phys. **71**, 2200161 (2023).
[52] S. Nesseris and J. Garcia-Bellido, A new perspective on dark energy modeling via genetic algorithms, J. Cosmol. Astropart. Phys. 11 (2012) 033.
[53] A. Gómez-Valent and L. Amendola, H_0 from cosmic chronometers and type Ia supernovae, with Gaussian processes and the novel weighted polynomial regression method, J. Cosmol. Astropart. Phys. 04 (2018) 051.
[54] D. M. Scolnic *et al.*, The complete light-curve sample of spectroscopically confirmed type Ia supernovae from Pan-STARRS1 and cosmological constraints from the combined Pantheon sample, arXiv:1710.00845.
[55] S. Cao, J. Ryan, and B. Ratra, Using Pantheon and DES supernova, baryon acoustic oscillation, and Hubble parameter data to constrain the Hubble constant, dark energy dynamics, and spatial curvature, Mon. Not. R. Astron. Soc. **504**, 300 (2021).
[56] R. Briffa, C. Escamilla-Rivera, J. Levi Said, and J. Mifsud, Constraints on f(T) cosmology with Pantheon+, Mon. Not. R. Astron. Soc. **522**, 6024 (2023).
[57] B. Gumjudpai, T. Naskar, M. Sami, and S. Tsujikawa, Coupled dark energy: Towards a general description of the dynamics, J. Cosmol. Astropart. Phys. 06 (2005) 007.
[58] G. Alestas, L. Kazantzidis, and L. Perivolaropoulos, $w-M$ phantom transition at $z_t < 0.1$ as a resolution of the Hubble tension, Phys. Rev. D **103**, 083517 (2021).
[59] D. W. Pesce *et al.*, The Megamaser Cosmology Project. XIII. Combined Hubble constant constraints, Astrophys. J. **891**, L1 (2020).
[60] S. Castello, M. Högås, and E. Mörtsell, A cosmological underdensity does not solve the Hubble tension, J. Cosmol. Astropart. Phys. 07 (2022) 003.
[61] G. Alestas, L. Kazantzidis, and L. Perivolaropoulos, H_0 tension, phantom dark energy, and cosmological parameter degeneracies, Phys. Rev. D **101**, 123516 (2020).
[62] L. Amendola and S. Tsujikawa, Phantom crossing, equation-of-state singularities, and local gravity constraints in $f(R)$ models, Phys. Lett. B **660**, 125 (2008).

[63] M. Libanov, V. Rubakov, E. Papantonopoulos, M. Sami, and S. Tsujikawa, UV stable, Lorentz-violating dark energy with transient phantom era, J. Cosmol. Astropart. Phys. 08 (2007) 010.

[64] L. Kazantzidis, L. Perivolaropoulos, and F. Skara, Constraining power of cosmological observables: Blind redshift spots and optimal ranges, Phys. Rev. D **99**, 063537 (2019).

[65] B. Sagredo, S. Nesseris, and D. Sapone, Internal robustness of growth rate data, Phys. Rev. D **98**, 083543 (2018).

[66] R. C. Nunes and S. Vagnozzi, Arbitrating the S_8 discrepancy with growth rate measurements from redshift-space distortions, Mon. Not. R. Astron. Soc. **505**, 5427 (2021).

[67] S. Basilakos, J. B. Dent, S. Dutta, L. Perivolaropoulos, and M. Plionis, Testing general relativity using the evolution of linear bias, Phys. Rev. D **85**, 123501 (2012).